Journal of The Electrochemical Society, **149** (12) A1533-A1540 (2002)
0013-4651/2002/149(12)/A1533/8/$7.00 © The Electrochemical Society, Inc.

Combined Effects of Ni and Li Doping on the Phase Transitions in Li_xCoO_2

Electrochemical and ^7Li Nuclear Magnetic Resonance Studies

S. Levasseur, M. Ménétrier, and C. Delmas*,z

Institut de Chimie de la Matière Condensée de Bordeaux-CNRS and Ecole Nationale Supérieure de Chimie et Physique de Bordeaux, 33608 Pessac cedex, France

High temperature $Li_{x_0}Co_{1-y}Ni_yO_2$ (x_0 = 1.0, 1.10; y = 0.0, 0.03, 0.06, and 0.10) phases were synthesized by solid-state chemistry. Their characterization by X-ray diffraction and galvanostatic measurements shows that 3% of Ni ions substituted for Co in the $LiCoO_2$ lattice suppress the two-phase domain, related to the semiconductor-to-metal transition, that is observed at the beginning of the charge process in Li_xCoO_2. These ions, trapped in the lattice, prevent the phase separation. On the other hand, more than 10% of Ni ions need to be substituted for Co in order to inhibit the monoclinic distortion due to a lithium/vacancy ordering in the interslab for $Li_{0.50}Co_{1-y}Ni_yO_2$. Besides, a Li/(Ni + Co) ratio (x_0) strictly higher than one in $Li_{x_0}Co_{0.97}Ni_{0.03}O_2$ leads, as in the case of the unsubstituted $Li_{1.10}CoO_2$ phase, to the disappearance of all the phase transitions upon deintercalation. ^7Li magic angle spinning nuclear magnetic resonance measurements show that Ni^{III} ions are the only paramagnetic species in the $LiCo_{1-y}Ni_yO_2$ phases while in the overlithiated $Li_{x_0}Co_{1-y}Ni_yO_2$ ($x_0 > 1.0$) phases, Ni^{III} and intermediate spin $Co^{3+(IS)}$ are present. This suggests the existence of structural defects associated with O vacancies which are responsible for the suppression of the electronic delocalization and of the lithium/vacancy ordering upon lithium deintercalation.
 [DOI: 10.1149/1.1516219]

Manuscript submitted December 31, 2001; revised manuscript received May 20, 2002. Available electronically October 18, 2002.

$LiCoO_2$ is the most widely used positive electrode material in commercial Li-ion batteries.[1,2] The high-temperature form of $LiCoO_2$ crystallizes in the trigonal system (space group: $R\bar{3}m$) with the ideal layered α-$NaFeO_2$ structure in which LiO_6 and CoO_6 octahedra share their edges and are stacked alternately along the c axis direction with an AB CA BC oxygen packing.[3] Numerous investigations have reported the phase changes upon lithium deintercalation in Li_xCoO_2, with the existence of a two-phase domain for $0.75 \leqslant x \leqslant 0.94$ due to a macroscopic semiconductor-to-metal transition and the presence of a monoclinic distortion for $x = 0.50$ due to the establishment of an interslab Li/vacancy ordering.[1,4-7] However, since the earliest work, in an effort to improve its electrochemical performances, substitution of numerous metallic elements for cobalt has been attempted (Cr,[8] Al,[9,10] Mg,[11,12] Fe,[13] or Mn[14,15]). However, only the derivatives of the mixed $LiCo_{1-y}Ni_yO_2$ oxide, for which a complete solid solution exists between the two end members $LiCoO_2$ and $LiNiO_2$, seem to be an interesting candidate from the electrochemical point of view.[5,16,17]

In this context, in 1993 Reimers *et al.* studied the effect of Ni doping in $LiCoO_2$. They showed that 2% of the nickel ions substituted for cobalt suppress the occurrence of the monoclinic distortion in $Li_{0.50}Co_{0.98}Ni_{0.02}O_2$ concluding that phase transitions are very sensitive to impurity levels and could be used as a quality control check on the material.[18] More recently, we observed that both phase transitions upon deintercalation can be suppressed as well in the unsubstituted lithium cobalt oxide by using nominal Li/Co ratios strictly higher than 1.0 in a high-temperature synthesis.[19]

In this general context, we performed a study on the combined effects of Ni doping and Li overstoichiometry in $LiCoO_2$. We synthesized $Li_{x_0}Co_{1-y}Ni_yO_2$ (x_0 = 1.0, 1.10; y = 0.0, 0.03, 0.06, and 0.10) materials and characterized them using X-ray diffraction (XRD), galvanostatic intercalation/deintercalation tests, and ^7Li magic angle spinning nuclear magnetic resonance (MAS NMR) spectroscopy.

Experimental

The $Li_{x_0}Co_{1-y}Ni_yO_2$ (x_0 = 1.0, 1.10; y = 0.0, 0.03, 0.06, and 0.10) materials were prepared by calcination at 600°C under O_2 for 12 h of Li_2Co_3 (Rhône Poulenc Rectapur % min 99), Co_3O_4 [calcination at 450°C for 12 h under O_2 of $Co(NO_3)_2 \cdot 6H_2O$ Carlo Erba % min 99], and NiO (calcination at 450°C for 12 h under O_2 of $Ni(NO_3)_2 \cdot 6H_2O$ Carlo Erba % min 99); x_0 denotes the nominal Li/(Co + Ni) ratio of the mixture; two compositions were considered in this study, x_0 = 1.0 and 1.10. Two successive heat-treatments at 900°C for 24 h with an intermediate grinding were done after the calcination.

Electrochemical measurements were carried out at room temperature (22°C) with Li/$LiClO_4$-propylene carbonate (PC)/$Li_xCo_{1-y}Ni_yO_2$ cells. The positive electrode consisted of a mixture of 88% by weight active material, 2% polytetrafluorethylene (PTFE), and 10% carbon black. The first series of cells, assembled in an argon-filled dry box, was charged at 100 $\mu A\ cm^{-2}$ (m_{LiCoO_2} = 30 mg); the second series, for long-range cycling, was cycled at 400 $\mu A\ cm^{-2}$ (m_{LiCoO_2} = 15 mg, C/20 rate). The $Li_xCo_{0.97}Ni_{0.03}O_2$ (x_0 = 1.0) deintercalated materials for XRD characterization were recovered in an argon-filled dry box, washed in dimethyl carbonate (DMC) and dried under vacuum.

The XRD patterns of the $Li_{x_0}Co_{1-y}Ni_yO_2$ starting materials were recorded using a Siemens D5000 powder diffractometer using the Cu Kα radiation and a graphite diffracted beam monochromator. Rietveld refinements were performed using the *Fullprof* program with a pseudo-Voigt fitting function.[20] XRD patterns of the $Li_xCo_{0.97}Ni_{0.03}O_2$ (x_0 = 1.0) deintercalated materials were recorded on a Philips PW1820 powder diffractometer using the Cu Kα radiation, in a special airtight holder under argon atmosphere in order to prevent any reaction with air moisture.

^7Li MAS NMR spectra were recorded on a Bruker MSL200 spectrometer at 77.7 MHz, with a standard 4 mm Bruker MAS probe. The samples were mixed with dry silica (typically 50% by weight), in order to facilitate the spinning and improve the field homogeneity, since they may exhibit metallic or paramagnetic properties. The mixture was placed into a 4 mm diam zirconia rotor in the dry box. Spinning speeds (υ_r) of 10 and 15 kHz were used. For all phases, a Hahn echo sequence [$t_{\pi/2} - \tau_1 - t_\pi - \tau_2$] was utilized in order to facilitate the phasing of all the signals and of their

* Electrochemical Society Active Member.
z E-mail: delmas@icmcb.u-bordeaux.fr

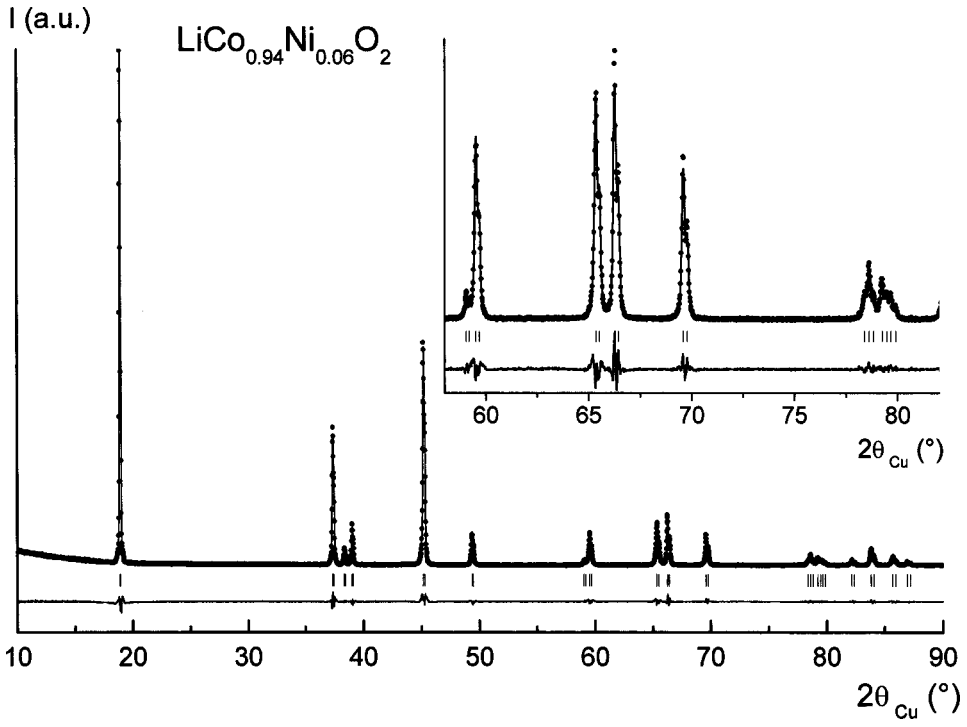

Figure 1. Observed and calculated XRD profiles for $Li_{1.0}Co_{0.94}Ni_{0.06}O_2$, filled circles: observed; solid line, calculated; lower trace, difference plot; bars, reflections.

spinning side bands and to ensure the observation of possibly very wide signals which would be lost during the receiver dead time in single pulse experiments. The 90° pulse duration used ($t_{\pi/2}$) was equal to 3.05 μs. In order to synchronize the spin echo with the first rotational echo, τ_1 was fixed to the rotor period $T_r = 1/\nu_r$. With such a Hahn echo sequence, phasing can be done easily, with only zero order correction if required, and no baseline correction is needed. A 200 kHz spectral width was used, and the recycle time $D_0 = 1$ s is long enough to avoid T_1 saturation effects. The isotropic shifts reported in parts per million are relative to an external sample of 1 M LiCl solution in water.

Since the purpose of this study is to emphasize the combined effect of Ni doping and Li overstoichiometry on the properties of $Li_x(Co,Ni)O_2$ phases, all the results reported in this work were obtained for the same batch for each $Li_{x_0}Co_{1-y}Ni_yO_2$ material. Furthermore, in order to control the reproducibility of the experimental results, two different batches of each material were characterized.

Table I. Rietveld refinement of the $Li_{1.0}Co_{0.94}Ni_{0.06}O_2$ XRD spectrum.

$Li_{1.0}Co_{0.94}Ni_{0.06}O_2$ S.G.: $R\bar{3}m$ $a_{hex.}$=2.8176(2) Å, $c_{hex.}$=14.062(1) Å

		Wyckoff positions				
Atom	Site	x	y	z	Occupancy	B (Å^2)
Li(1)	3b	0	0	1/2	1.0	0.51(40)
Co(1)	3a	0	0	0	0.94	−0.04(8)
Ni(1)	3a	0	0	0	0.06	−0.04(8)
O	6c	0	0	0.2597(5)	1.0	0.05(16)

Profile function: pseudo-Voigt $PV = \eta L + (1 - \eta)G$; $\eta = \eta_0 + X(2\theta)$ $U = 0.025(8)$, $V = 0.013(4)$, $W = 0.005(1)$; $\eta_0 = 0.23(4)$, $X = 0.004(1)$.

Conventional Rietveld factors: $R_{wp} = 13.4$, $R_B = 2.85$, $\chi^2 = 4.78$, 14 refined parameters.

The standard deviations were multiplied by the Scor parameter (=4) to correct for local correlations.

Results and Discussion

X-ray diffraction study. Rietveld refinements.—All the starting $Li_{x_0}Co_{1-y}Ni_yO_2$ materials were characterized by XRD. In all cases, pure phases are obtained without any trace of synthesis reactants or parasitic phases. All materials exhibit narrow diffraction lines whatever the percentage of nickel ions in the structure. They crystallize in the trigonal system (space group: $R\bar{3}m$), with the ideal α-$NaFeO_2$ layered structure of HT-$LiCoO_2$. Since the XRD patterns are very similar and close to those reported in the literature for the $LiCo_{1-y}Ni_yO_2$ system,[5,16,17,21] only that of the $LiCo_{0.94}Ni_{0.06}O_2$ material is shown in Fig. 1.

All the $Li_{x_0}Co_{1-y}Ni_yO_2$ samples were characterized by Rietveld refinement of powder XRD data. As the morphology of the crystallites could influence the line intensity ratios on diffraction patterns, all the Rietveld samples were prepared in such a way that preferred orientation was minimized.[22] The refinement was led, in a first step, using a strictly 2D model. Global occupancies for the 3a [$(1 - y)$Co + yNi], 3b (Li), and 6c (O) sites were fixed to 1.0. Due to Co absorption, the release of the occupancy values of the 3a and 3b sites always leads to a decrease of the Co/Ni (3a) site occupancy, no significant change in the occupancy value for the Li 3b

Table II. Hexagonal cell parameters and oxygen z position from refinement of XRD patterns for the various $Li_{x_0}Co_{1-y}Ni_yO_2$ phases.

Sample	$a_{hex.}$ (Å)	$c_{hex.}$ (Å)	z_{ox}[a]	c/a
$Li_{1.0}CoO_2$[b]	2.81506(16)	14.0516(8)	0.2603(4)	4.99
$Li_{1.0}Co_{0.97}Ni_{0.03}O_2$	2.8177(1)	14.056(1)	0.2582(9)	4.99
$Li_{1.0}Co_{0.94}Ni_{0.06}O_2$	2.8176(2)	14.062(1)	0.2597(5)	4.99
$Li_{1.0}Co_{0.90}Ni_{0.10}O_2$	2.8182(2)	14.067(1)	0.2584(9)	4.99
$Li_{1.10}CoO_2$[b]	2.81605(18)	14.0511(8)	0.2593(6)	4.99
$Li_{1.10}Co_{0.97}Ni_{0.03}O_2$	2.8172(1)	14.058(1)	0.2597(7)	4.99

[a] 6c oxygen z position.
[b] Ref. 19.

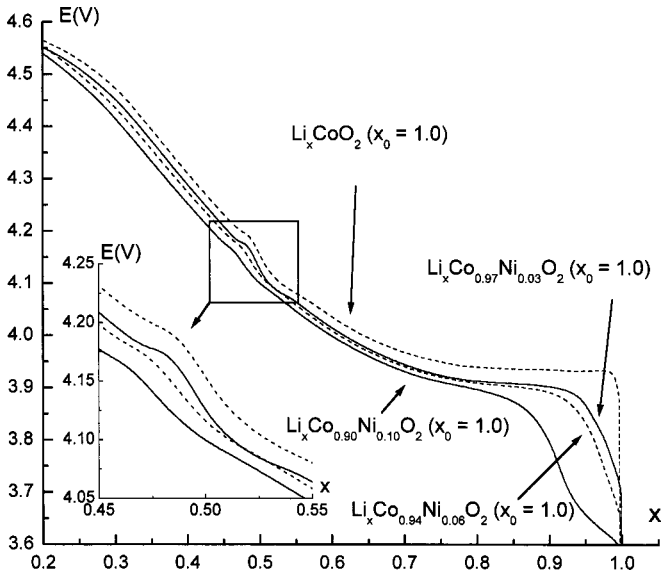

Figure 2. First galvanostatic charge of $Li//Li_xCo_{1-y}Ni_yO_2$ (x_0 = 1.0, y = 0.0, 0.03, 0.06, and 0.10) electrochemical cells (J = 100 μA cm^{-2}; $m_{Li(CoNi)O_2}$ = 30 mg).

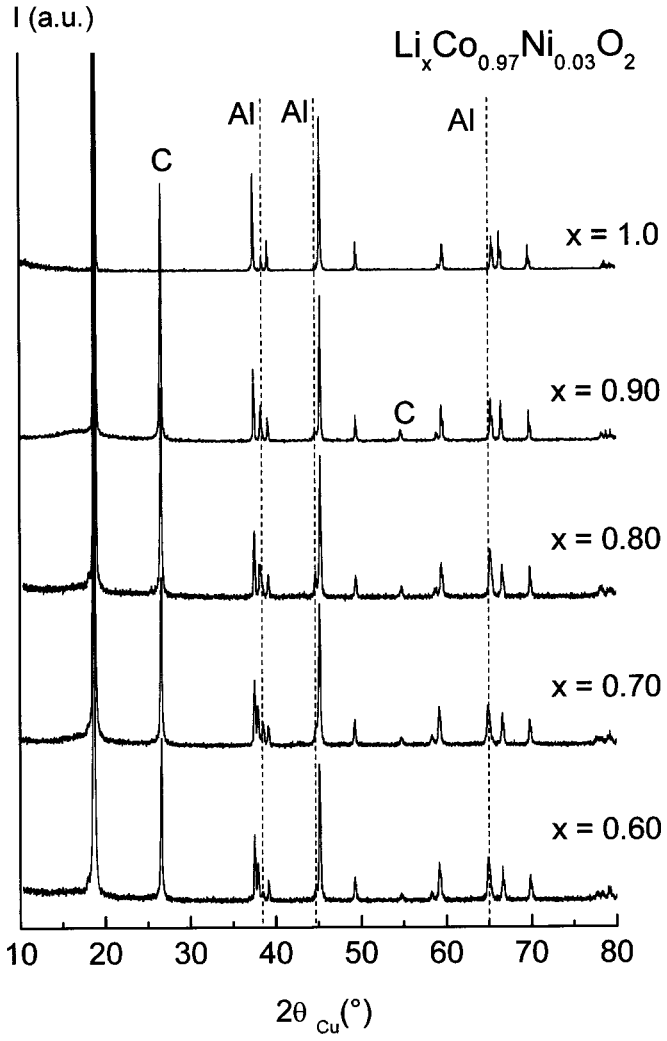

Figure 3. XRD patterns of the electrochemically deintercalated $Li_xCo_{0.97}Ni_{0.03}O_2$ (x_0 = 1.0) samples (0.60 ⩽ x ⩽ 1.0).

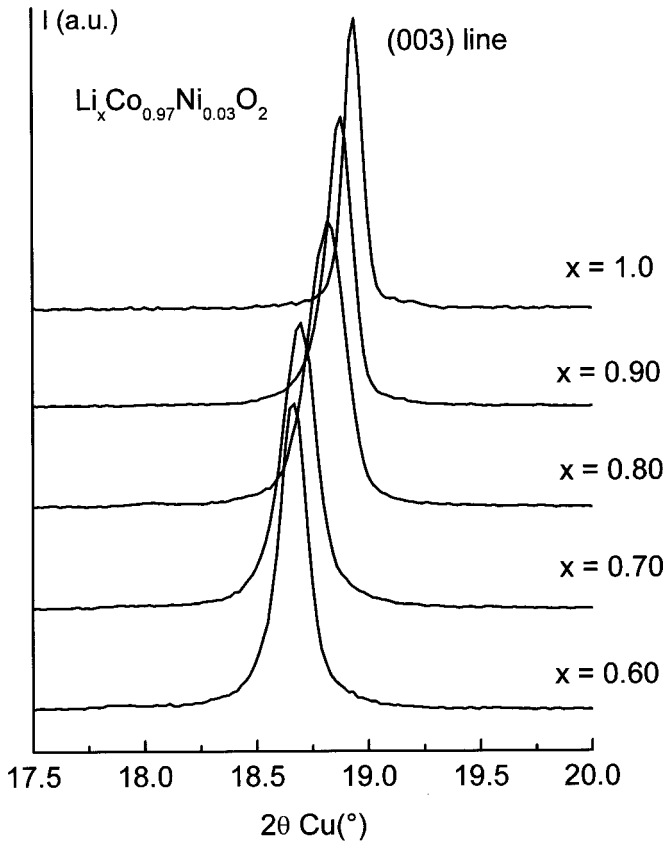

Figure 4. Expansion of the (003) Bragg reflection of the XRD patterns of the electrochemically deintercalated $Li_xCo_{0.97}Ni_{0.03}O_2$ (x_0 = 1.0) samples (0.60 ⩽ x ⩽ 1.0).

site being observed. The results are presented in Table I for the $LiCo_{0.94}Ni_{0.06}O_2$ phase and are in agreement with the structural data reported for pure 2D-$LiCo_{1-y}Ni_yO_2$ (y ⩽ 0.70) phases by Rougier *et al.*[21] In our $Li_{x_0}Co_{1-y}Ni_yO_2$ phases, the hypothesis of a fraction of Co and/or Ni ions in the lithium 3b site is rejected since the fits invariably lead to a negative occupancy. However, due to the impossibility of quantifying Co absorption in the Bragg-Brentano geom-

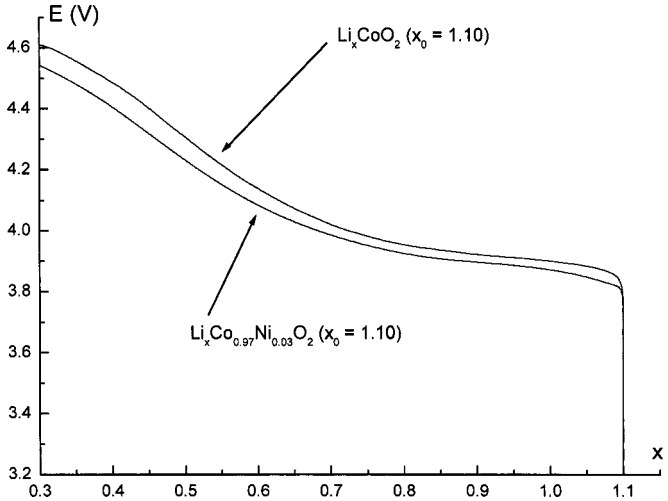

Figure 5. First galvanostatic charge of $Li//Li_xCo_{1-y}Ni_yO_2$ (x_0 = 1.10, y = 0.0, 0.03) electrochemical cells (J = 100 μA cm^{-2}; $m_{Li(Co,Ni)O_2}$ = 30 mg).

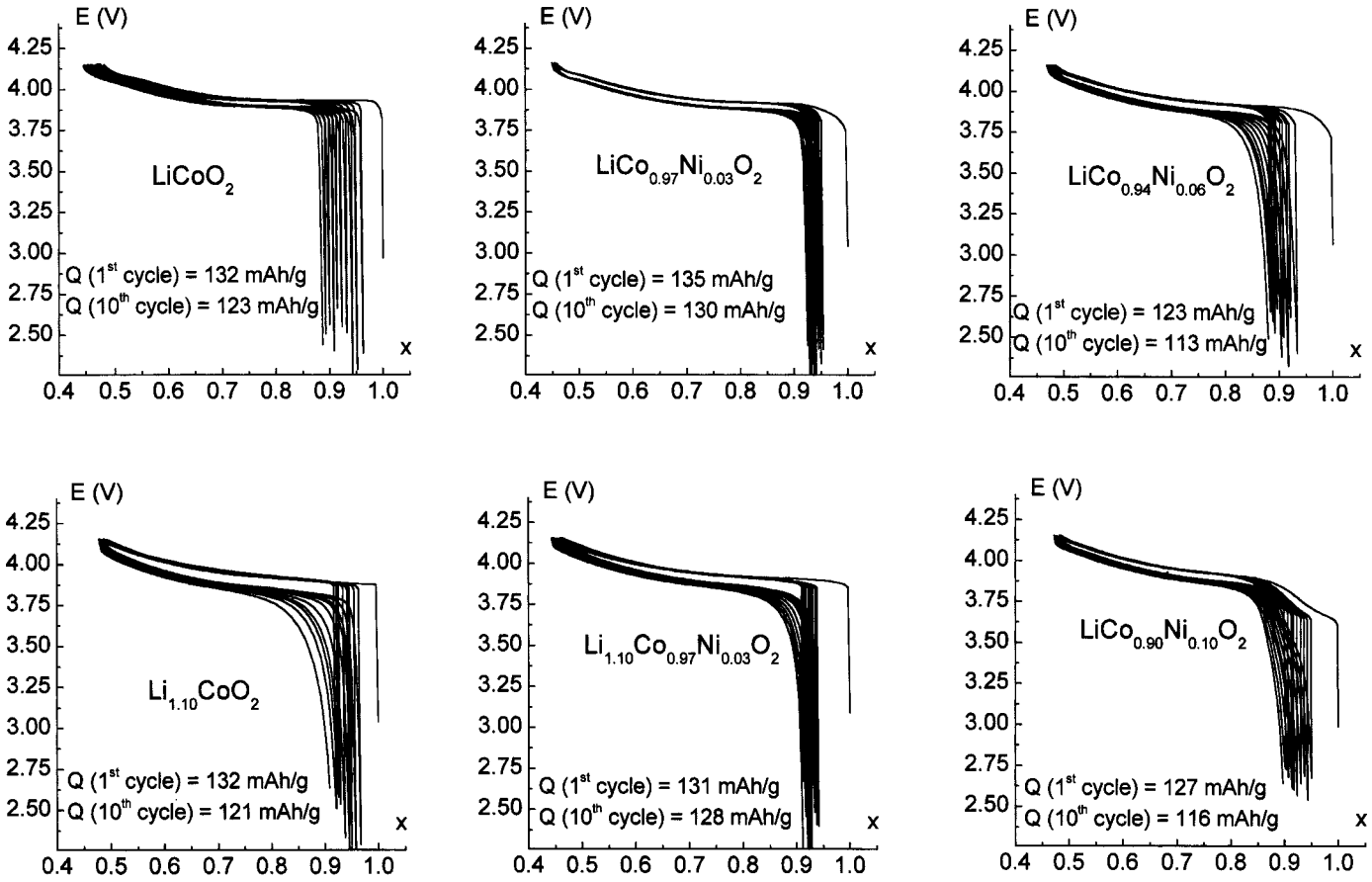

Figure 6. Cycling behavior of the various Li//$Li_xCo_{1-y}Ni_yO_2$ (x_0 = 1.0, 1.10; y = 0.0, 0.03, 0.06, and 0.10) electrochemical cells (J = 400 μA cm^{-2}; $m_{Li(Co,Ni)O_2}$ = 15 mg, C/20 rate) between 2.7 and 4.15 V.

etry, no conclusion could be drawn about the presence of Li ions in the 3a crystallographic site of Co/Ni. Nevertheless, in agreement with the previous neutron diffraction studies on pure $LiCoO_2$, one can consider the amount of Li^+ ions in the Co/Ni 3a site as negligible.[3,19] The very good fitting of the profile of the XRD lines and the small intensity of the line in the difference pattern emphasize the quality of the Rietveld refinement.

The structural parameters of the various $Li_{x_0}Co_{1-y}Ni_yO_2$ materials are presented in Table II. Both the $a_{hex.}$ and the $c_{hex.}$ parameters increase smoothly with Ni doping due to the difference in size between the trivalent nickel and cobalt ions ($r_{Ni^{III}}$ = 0.56 Å, $r_{Co^{III}}$ = 0.545 Å[23]). Furthermore, in all materials, the $c_{hex.}/a_{hex.}$ ratio close to five ($\neq$4.90 for a cubic lattice) confirms the 2D character of the structure of the Ni-doped $LiCoO_2$ phases,[21,24] in good agreement with the high and constant value of the oxygen z position ($z_{ox.}$) and the consequent difference in the slab (S) and interslab space (I) thicknesses (S = 2.06 Å $\neq$ I = 2.63 Å for $Li_{x_0}Co_{1-y}Ni_yO_2$ phases).[25]

Electrochemical Study

Lithium-stoichiometric $LiCo_{1-y}Ni_yO_2$ phases (y = 0.0, 0.03, 0.06, and 0.10).—Figure 2 shows the first galvanostatic charge curve of Li//$Li_xCo_{1-y}Ni_yO_2$ cells (x_0 = 1.0; y = 0.0, 0.03, 0.06, and 0.10) at low rate [J = 100 μA cm^{-2}, $m_{Li(Co,Ni)O_2}$ = 30 mg; C/160 rate (160 h are required to exchange one equivalent of electron)].

As already reported, the charge curve obtained with the pure Li_xCoO_2 (x_0 = 1.0) material exhibits both the voltage plateau at *ca.* 3.93 V corresponding to the biphasic domain for 0.75 $\leqslant$ x $\leqslant$ 0.94 due to a semiconductor-to-metal transition and the particular feature associated to the monoclinic distortion expected for $Li_{0.50}CoO_2$ due to the interslab lithium/vacancy ordering.[4,7]

A quite different behavior is observed for the Ni-doped materials. In the first part of the oxidation of the $LiCo_{1-y}Ni_yO_2$ ($y > 0$) phases, the preferential oxidation of Ni ions compared to Co ones leads to the appearance of a lower potential step, all the more pronounced when the nickel amount increases. This difference in potential is due to the lower oxidizing power of the Ni^{III}/Ni^{IV} redox couple compared to the Co^{III}/Co^{IV} one.[17,26] Moreover, the voltage plateau at the beginning of the charge process is less marked for the Ni-doped materials, even with only 3% of the doping element in the $LiCoO_2$ lattice, suggesting that the two-phase domain does not exist anymore in these materials. This is fully confirmed by the XRD patterns of electrochemically deintercalated $Li_xCo_{0.97}Ni_{0.03}O_2$ materials; as shown in Fig. 3 and 4, a solid solution is obtained for 0.60 $\leqslant$ x $\leqslant$ 1.0 in the $Li_xCo_{0.97}Ni_{0.03}O_2$ (x_0 = 1.0) system. One can see in Fig. 2 that the monoclinic distortion for x = 0.50 exists in all the $Li_xCo_{1-y}Ni_yO_2$ (y = 0.0, 0.03, 0.06, and 0.10) systems studied here. This result conflicts with the conclusion by Reimers *et al.* who showed in a former study that 2% of the Ni ions substituted for cobalt are sufficient to suppress the monoclinic distortion at room temperature.[18] Besides, one can see on the inset of Fig. 2 that this order/disorder transition tends to disappear for Ni contents higher than 10%.

Lithium overstoichiometric $Li_{1.10}Co_{1-y}Ni_yO_2$ phases (y = 0.0 and 0.03).—Contrary to the case of the Li stoichiometric materials, as shown in Fig. 5, the first galvanostatic charge curves of Li//$Li_xCo_{1-y}Ni_yO_2$ cells (x_0 = 1.10; y = 0.0 and 0.03) at a low

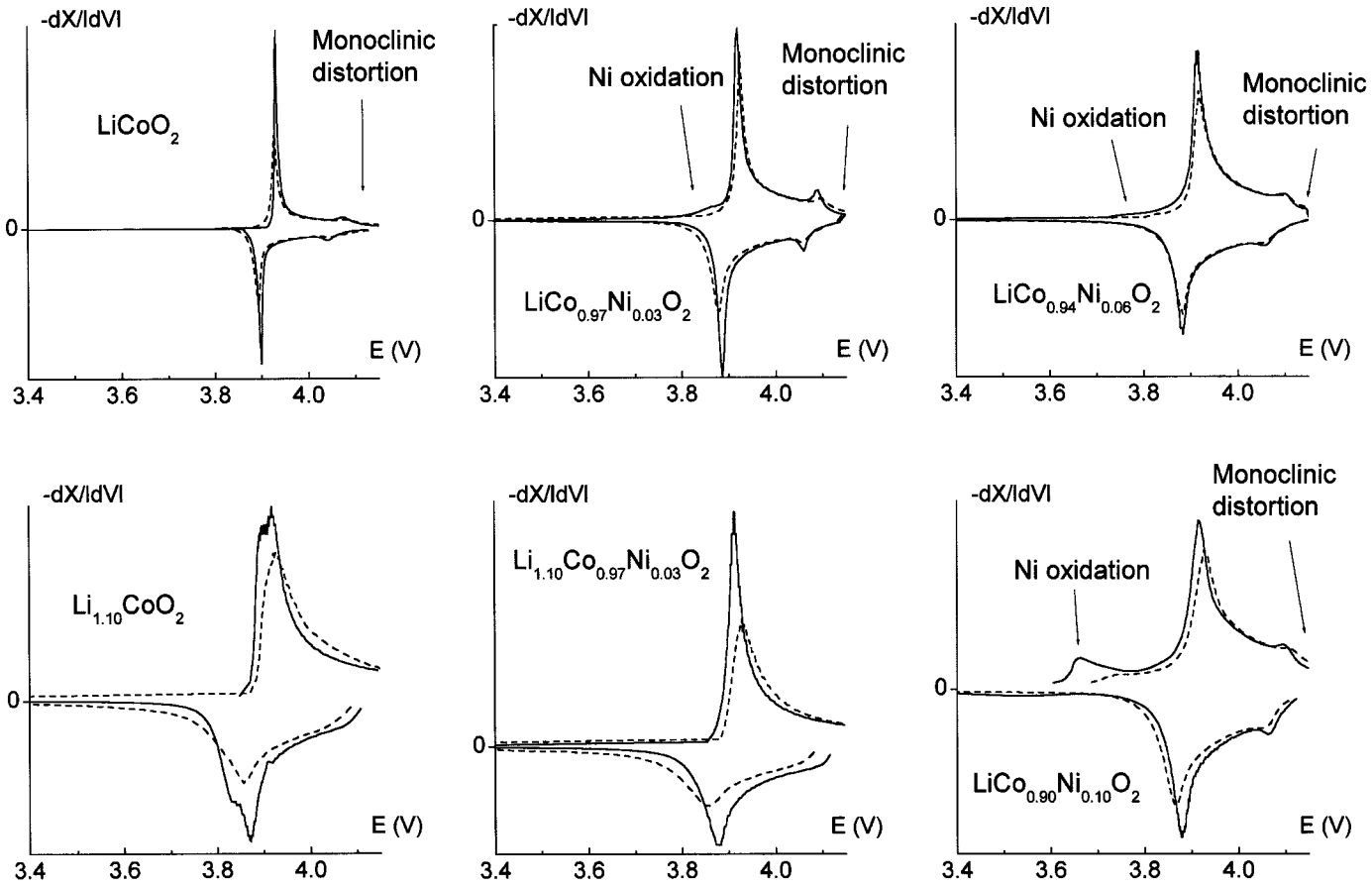

Figure 7. $-dx/|dV| = f(V)$ derivatives curves of the first (solid line) and 10th (dashed line) cycles of the various Li//$Li_xCo_{1-y}Ni_yO_2$ (x_0 = 1.0, 1.10; y = 0.0, 0.03, 0.06, and 0.10) electrochemical cells (J = 400 μA cm^{-2}; $m_{Li(CoNi)O_2}$ = 15 mg) between 2.7 and 4.15 V.

rate (J = 100 μA cm^{-2}, $m_{Li(Co,Ni)O_2}$ = 30 mg, C/180 charging rate) have a quite similar profile, whatever the value of y. The feature corresponding to the monoclinic distortion for x = 0.50 and the voltage plateau at the beginning of the charge have disappeared both for the Ni-doped and for the pure $Li_{1.10}CoO_2$ phases. The unidirectional increase of the potential during lithium deintercalation suggests the occurrence of a monophasic reaction throughout the charge process for the $Li_{1.10}Co_{1-y}Ni_yO_2$ materials. An XRD study of electrochemically deintercalated Li_xCoO_2 (x_0 = 1.10) materials carried out in a former work had confirmed such an observation.[19] The same behavior is expected for the $Li_{1.10}Co_{0.97}Ni_{0.03}O_2$ system, although no XRD characterization was performed on deintercalated materials.

Cycling tests.—Li/$LiClO_4$-PC/$Li_{x_0}Co_{1-y}Ni_yO_2$ (x_0 = 1.0, 1.10; y = 0.0, 0.03, 0.06, and 0.10) cells were cycled between 2.7 and 4.15 V at 400 μA cm^{-2} (C/20 rate) as shown in Fig. 6. The reversible capacity for the first and tenth cycle is also indicated on the figure. The purpose of this study is to characterize the structural transitions and not to obtain large reversible capacities, a relatively low high-voltage cutoff was used.

As already reported elsewhere, the cycling behavior of the Co-rich $Li_xCo_{1-y}Ni_yO_2$ phases is very satisfactory and close to that of pure $LiCoO_2$.[16,24] The cycling curves, on Fig. 6, show that the reversibility of the deintercalation/intercalation process is good, as the reversible capacities for the first and tenth cycles, shown in Fig. 6, are quite high in the voltage window used. Note that the slight decrease in potential caused by 3% doping of Ni leads to a particularly good cycling capacity for the cutoff voltage used (4.15 V). Furthermore, one can note that polarization is very small in all cases and that the irreversible capacity at the first cycle is especially low compared to that of the $LiNiO_2$-type compounds.[27]

The derivative curves $-dx/|dV| = f(V)$ of the first and tenth cycles of the Li//$Li_{x_0}Co_{1-y}Ni_yO_2$ cells presented just above are reported in Fig. 7. One can note the peak at the lower potential due to the preferential oxidation of Ni^{III} ions compared to Co^{III} ones at the beginning of the charging process. Furthermore, as already evidenced from the slow rate charging curves (Fig. 2), the trace of the monoclinic distortion around 4.15 V is easily observable in all the cycling curves from the Li stoichiometric $LiCo_{1-y}Ni_yO_2$ phases and still exists after ten cycles, confirming the persistence of an order/disorder transition for x = 0.50 in these materials. On the contrary, it does not appear for lithium overstoichiometric materials.

^{7}Li MAS NMR Study

^{7}Li MAS NMR spectroscopy measurements were carried out on the various $Li_{x_0}Co_{1-y}Ni_yO_2$ starting materials. Figures 8 and 9 show the 15 kHz ^{7}Li MAS NMR spectra of the lithium-stoichiometric $LiCo_{1-y}Ni_yO_2$ materials (y = 0.0, 0.03, and 0.06) and of the Li overstoichiometric $Li_{1.10}Co_{0.97}Ni_{0.03}O_2$ phase.

As already reported, $LiCoO_2$ exhibits a single narrow signal close to 0 ppm due to the exclusive presence of diamagnetic low spin Co^{III} ions in the structure, so that no hyperfine interaction is expected.[28,29] For lithium stoichiometric Ni-doped materials, three new signals at 110, −15, and −30 ppm are observed. These signals have been attributed by Marichal *et al.* to the presence of paramagnetic low spin Ni^{III} ions with one single electron in the e_g orbital ($t_{2g}^6e_g^1$). The transfer of hyperfine interaction between the single e_g electron toward the surrounding lithium ions can be done via the

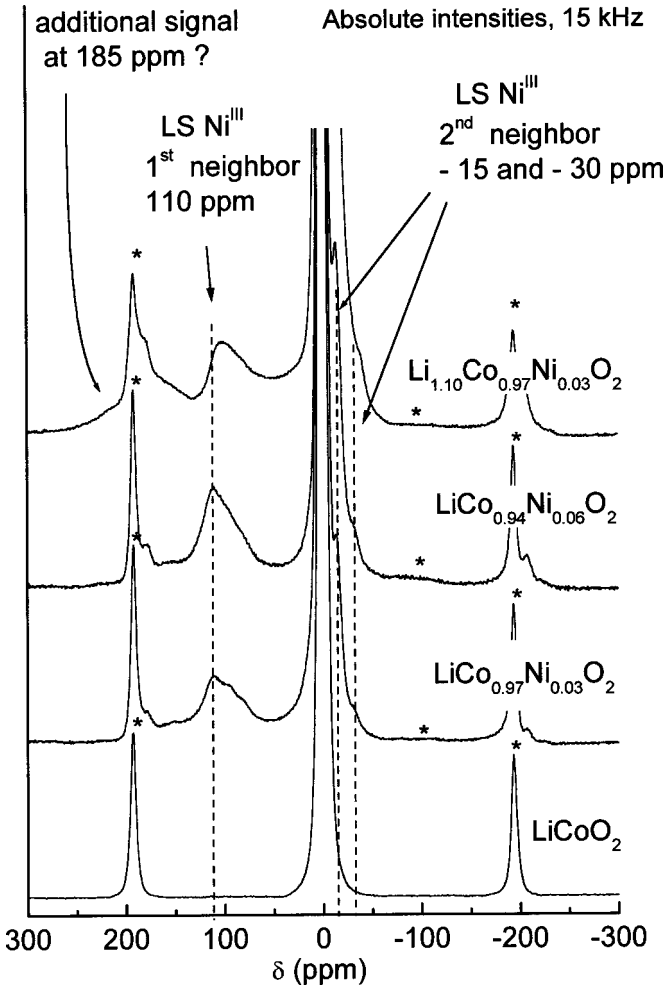

Figure 8. 15 kHz ^{7}Li MAS NMR spectra for the various $Li_{x_0}Co_{1-y}Ni_yO_2$ phases (x_0 = 1.0, 1.10; y = 0.0, 0.03, 0.06), (* = spinning side bands).

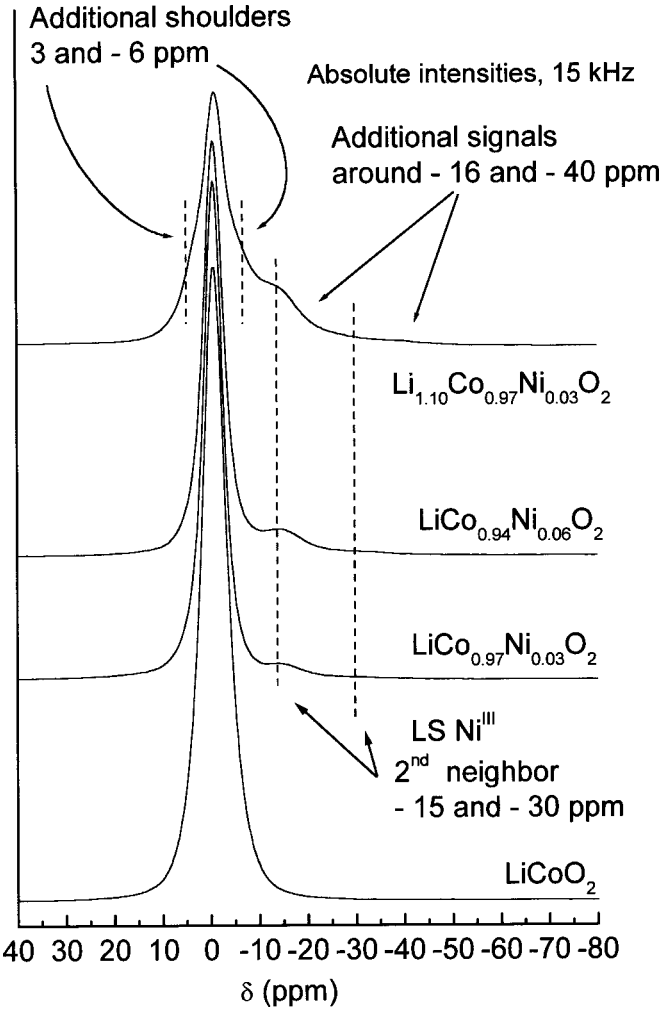

Figure 9. Expansion of the central signal of 15 kHz ^{7}Li MAS NMR spectra for the various $Li_{x_0}Co_{1-y}Ni_yO_2$ phases (x_0 = 1.0, 1.10; y = 0.0, 0.03, 0.06).

overlap with the oxygen orbitals with a 90° (first neighbor) or 180° geometry (second neighbor). The 110 ppm signal is assigned to Li ions with one Ni^{III} ions as the first neighbor while the −15 and −30 ppm signals result from the presence of Li ions with one and two Ni^{III} ions as the second neighbor, respectively.[26,29] As expected, the magnitude of the Ni^{III} ions signals is all the more pronounced since the percentage of Ni ions in the material is large.

Furthermore, one can observe in Fig. 9 that the central signal of the $Li_{1.10}Co_{0.97}Ni_{0.03}O_2$ material is quite different from those of the lithium stoichiometric Ni-doped phases, showing characteristic shoulders centered approximately at 3 and −6 ppm. These features are similar to those observed in the case of the $Li_{1.10}CoO_2$ phase (see Fig. 11), resulting from the presence of a structural defect leading to oxygen vacancies in the material. In $Li_{1.10}CoO_2$, these signals, initially attributed to the presence of divalent cobalt ions, are in fact due to Li^+ ions in the vicinity of paramagnetic trivalent cobalt ions in a quite unusual spin state.[19,30] Indeed, this structural defect, induced by a nominal Li excess during the synthesis, leads to the presence of intermediate spinning Co^{3+} ions (labeled $Co^{3+(IS)}$) which are responsible for three characteristic first/second neighbor effect NMR signals at 185 ppm (one $Co^{3+(IS)}$ first neighbor) and −16 and −40 ppm (one and two $Co^{3+(IS)}$ second neighbor, respectively). Furthermore, the two shoulders on the 0 ppm signal (3 and −6 ppm) are considered to be due to Li^+ ions in an oxygen environment perturbed by the oxygen vacancy, leading to various mechanisms of transfer of the hyperfine interaction from the Li^+ ion close to the oxygen vacancy. These shoulders are clearly apparent in the spectra of the $Li_{1.10}Co_{0.97}Ni_{0.03}O_2$.[19] However, since the −16 and −40 ppm $Co^{3+(IS)}$ signals must get mixed up with the −15 and −30 ppm Ni^{III} signals and because the first spinning side band must hide the possible presence of a signal at 185 ppm, one cannot clearly observe these signals on the 15 kHz MAS spectra.

As concerns the first-neighbor effect of $Co^{3+(IS)}$ ions in $Li_{1.10}Co_{0.97}Ni_{0.03}O_2$, the first spinning side band at ±190 ppm is clearly superposed on another band in the case of the lithium overstoichiometric material (Fig. 8). Therefore, in order to better observe the 150/250 ppm range, we have performed MAS NMR measurements using a 10 kHz rotation speed to shift the spinning side band without modifying the isotropic shifts. The NMR spectra, shown in Fig. 10 and compared to that of the $Li_{1.10}CoO_2$ phase clearly show the signal associated with $Co^{3+(IS)}$ at 185 ppm for the $Li_{1.10}Co_{0.97}Ni_{0.03}O_2$ material. The expansion of the central signal of the various compounds (Fig. 11) confirms the presence of both Ni^{III} and $Co^{3+(IS)}$ ions in the lithium overstoichiometric $Li_{1.10}Co_{0.97}Ni_{0.03}O_2$ phase, the contribution of each type of paramagnetic ion adding in the −40/10 ppm range and leading to a loss in the central signal definition.

Conclusions

The galvanostatic measurements and XRD results allow us to point out some conclusions on the influence of Ni doping and Li

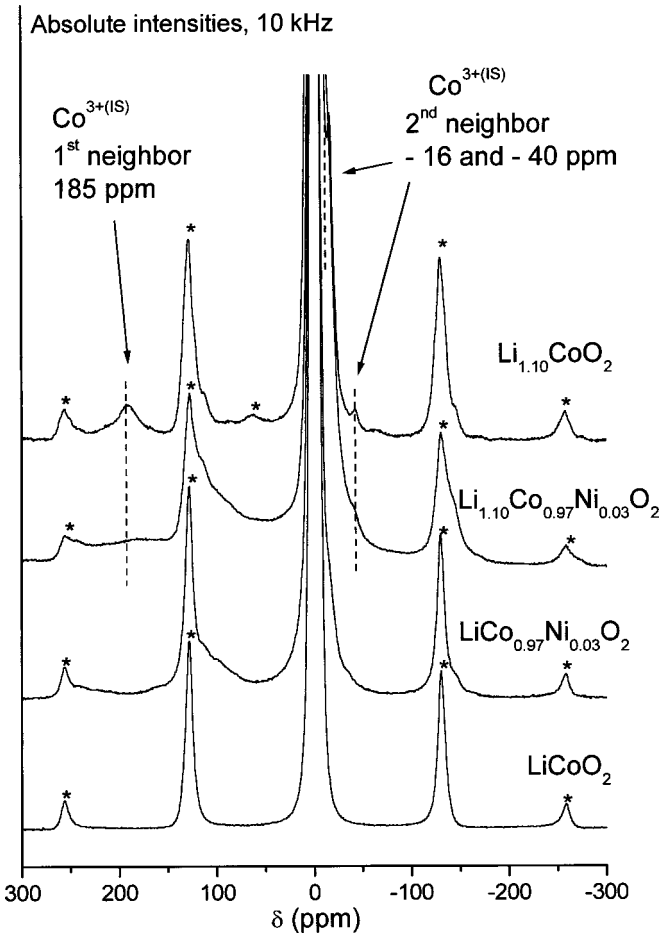

Figure 10. 10 kHz ^{7}Li MAS NMR spectra for the various $Li_{x_0}Co_{1-y}Ni_yO_2$ phases (x_0 = 1.0, 1.10; y = 0.0, 0.03), (* = spinning side bands).

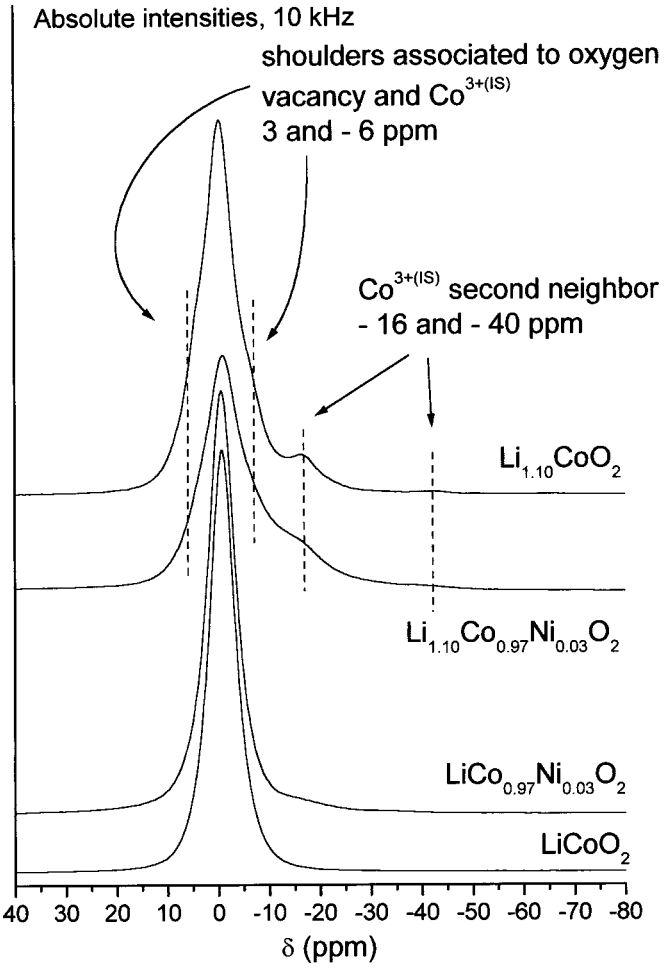

Figure 11. Expansion of the central signal of 10 kHz ^{7}Li MAS NMR spectra for the various $Li_{x_0}Co_{1-y}Ni_yO_2$ phases (x_0 = 1.0, 1.10; y = 0.0, 0.03).

nonstoichiometry in HT-$LiCoO_2$. This study clearly allows us to separate the relative effects of Ni-doping and lithium overstoichiometry which was not considered by Reimers *et al.*[18] We show here that 3% of Ni ions substituted for Co do not make the monoclinic distortion disappear.

Before any conclusion, we have to consider what are the driving forces for the phase transitions in the pure Li_xCoO_2 (x_0 = 1.0) system. On the one hand, it is now totally admitted that the biphasic domain for $0.75 \leqslant x \leqslant 0.94$ results from a brutal change in the electronic properties of the Li_xCoO_2 system as it undergoes a semiconductor-to-metal transition at the macroscopic scale.[7] On the other hand, the monoclinic distortion for x = 0.50 is considered to have a structural origin related to the establishment of a Li/vacancy ordering in the interslab layer.[4] Indeed, a recent TEM study clearly showed, for the first time, the Li/vacancy ordering in the monoclinic $Li_{0.50}CoO_2$ phase.[31] In the $Li_{x_0}CoO_2$ system ($x_0 > 1.0$), the presence of structural defects (oxygen vacancy associated to $Co^{3+(IS)}$ ions) induces enough perturbations in the slab to prevent any Li/vacancy ordering in the interslab space.[30] From the electronic properties point of view, even if the semiconductor-to-metal transition is observed upon lithium deintercalation, this transition is not associated with a phase separation since the defects are trapped in the lattice and cannot move at room temperature.

In the case of Ni-doped materials synthesized without any lithium excess, the experimental results show first that 6% of Ni ions substituted for Co do not create sufficient perturbations in the $(Co,Ni)O_2$ slab ordering to prevent the lithium/vacancy ordering in the insterlab and the resulting monoclinic distortion because of the close ionic radii of the Ni^{IV} and Co^{III} ions.[23] When 10% of Ni are substituted for Co, the effect becomes significant and the trace of the monoclinic distortion becomes weak. As a possible explanation of the discrepancy between our and Reimers's results on that point, we suggest that the Ni-substituted samples studied by this author may have been slightly Li-overstoichiometric.

Second, from the electronic properties point of view, the Ni ions are trapped in the lattice and are an obstacle to electron delocalization. Therefore, the expected phase separation associated with the semiconductor-to-metal transition cannot occur; a solid solution domain is observed upon lithium deintercalation. The behavior resulting from the presence of the nickel ions is very similar to that due to the structural defects associated with lithium overstoichiometry in the $Li_{x_0}CoO_2$($x_0 > 1.0$) phases.[19,30]

When both type of defects are simultaneously present (Ni ions and defects related to lithium overstoichiometry) as shown by NMR measurements conducted on the $Li_{1.10}Co_{0.97}Ni_{0.03}O_2$ phase, all the phase transitions disappear.

Finally, the NMR measurements show that the doping effects of nickel and lithium are cumulative and independent. Indeed, in the $Li_{1.10}Co_{0.97}Ni_{0.03}O_2$ phase, both $Co^{3+(IS)}$ ions (associated to an oxygen vacancy) and Ni^{III} ions coexist in the diamagnetic Co^{III} lattice.

Acknowledgments

The authors thank I. Saadoune, A. Audemer, L. Gautier, and J. Scoyer for fruitful discussions, and Umicore, ANRT, and Région Aquitaine for financial support.

Institut de Chimie de la Matière Condensée de Bordeaux assisted in meeting the publication costs of this article.

References

1. K. Mizushima, P. C. Jones, P. J. Wiseman, and J. B. Goodenough, *Mater. Res. Bull.*, **15**, 783 (1980).
2. H. Abe, K. Zaghib, K. Tatsumi, and S. Higuchi, *J. Power Sources*, **54**, 236 (1995).
3. H. J. Orman and P. J. Wiseman, *Acta Crystallogr., Sect. C: Cryst. Struct. Commun.*, **1984**, 12.
4. J. N. Reimers and J. R. Dahn, *J. Electrochem. Soc.*, **139**, 2091 (1992).
5. T. Ohzuku and A. Ueda, *J. Electrochem. Soc.*, **141**, 2972 (1994).
6. G. G. Amatucci, J. M. Tarascon, and L. C. Klein, *J. Electrochem. Soc.*, **143**, 1114 (1996).
7. M. Ménétrier, I. Saadoune, S. Levasseur, and C. Delmas, *J. Mater. Chem.*, **9**, 1135 (1999).
8. C. D. W. Jones, E. Rossen, and J. R. Dahn, *Solid State Ionics*, **68**, 65 (1994).
9. R. Alcantara, P. Lavela, P. L. Relano, J. L. Tirado, E. Zhecheva, and R. Stoyanova, *Inorg. Chem.*, **37**, 264 (1998).
10. Y. I. Jang, B. Huang, H. Wang, G. R. Maslkaly, G. Ceder, D. R. Sadoway, Y. M. Chiang, H. Liu, and H. Tamura, *J. Power Sources*, **81-82**, 589 (1999).
11. H. Tukamoto and A. R. West, *J. Electrochem. Soc.*, **144**, 3164 (1997).
12. E. Antolini, L. Giorgi, and M. Carewska, *J. Mater. Sci. Lett.*, **18**, 325 (1999).
13. H. Kobayachi, H. Shigemura, M. Tabuchi, H. Sakaebe, K. Ado, H. Kageyama, A. Hirano, R. Kanno, M. Wakita, S. Morimoto, and S. Nasu, *J. Electrochem. Soc.*, **147**, 960 (2000).
14. R. Stoyanova, E. Zhecheva, and L. Zarkova, *Solid State Ionics*, **73**, 233 (1994).
15. S. Waki, K. Dokko, T. Itoh, M. Nishizawa, T. Abe, and I. Uchida, *J. Solid State Electrochem.*, **4**, 205 (2000).
16. C. Delmas, I. Saadoune, and A. Rougier, *J. Power Sources*, **43-44**, 595 (1993).
17. I. Saadoune and C. Delmas, *J. Mater. Chem.*, **6**, 193 (1996).
18. J. N. Reimers, J. R. Dahn, and U. Von Sacken, *J. Electrochem. Soc.*, **140**, 2752 (1993).
19. S. Levasseur, M. Ménétrier, E. Suard, and C. Delmas, *Solid State Ionics*, **128**, 11 (2000).
20. J. Rodriguez-Carvajal, in *Fullprof*, Laboratoire L. Brillouin (CEA-CNRS), http://www-llb.cea.fr/fullweb/powder.htm (1990).
21. A. Rougier, I. Saadoune, P. Gravereau, P. Willmann, and C. Delmas, *Solid State Ionics*, **90**, 83 (1996).
22. L. B. Mccusker, R. B. Von Dreele, D. E. Cox, D. Louer, and P. Scardi, *J. Appl. Crystallogr.*, **32**, 36 (1999).
23. R. D. Shannon and C. T. Prewitt, *J. Appl. Crystallogr.*, **25**, 925 (1969).
24. I. Saadoune, M. Ménétrier, and C. Delmas, *J. Mater. Chem.*, **7**, 2505 (1997).
25. A. Rougier, P. Gravereau, and C. Delmas, *J. Electrochem. Soc.*, **143**, 1168 (1996).
26. D. Carlier, M. Ménétrier, and C. Delmas, *J. Mater. Chem.*, **11**, 594 (2001).
27. J. P. Pérès, C. Delmas, A. Rougier, M. Broussely, F. Perton, P. Biensan, and P. Willmann, *J. Phys. Chem. Solids*, **57**, 1057 (1996).
28. M. Ménétrier, A. Rougier, and C. Delmas, *Solid State Commun.*, **90**, 439 (1994).
29. C. Marichal, J. Hirschinger, P. Granger, M. Ménétrier, A. Rougier, and C. Delmas, *Inorg. Chem.*, **34**, 1773 (1995).
30. S. Levasseur, M. Ménétrier, L. Gautier, A. Audemer, G. Demazeau, A. Largeteau, and C. Delmas, *J. Mater. Chem.*, Submitted (2001).
31. Y. Shao Horn, F. Weill, S. Levasseur, and C. Delmas, To be published.